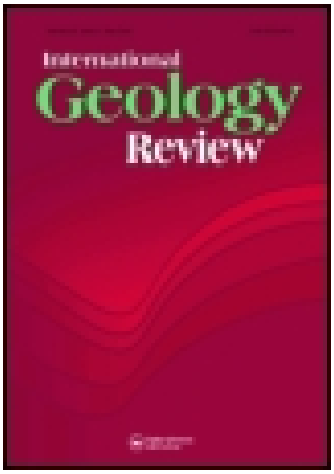

International Geology Review
Publication details, including instructions for authors and subscription information:
http://www.tandfonline.com/loi/tigr20

Serpentines Close-Up and Intimate: An HRTEM View

István Dódony [a] & Peter R. Buseck [a]
[a] Arizona State University
Published online: 14 Jul 2010.

International Geology Review, Vol. 46, 2004, p. 507–527.

Serpentines Close-Up and Intimate: An HRTEM View

ISTVÁN DÓDONY[1] AND PETER R. BUSECK[2]

Departments of Geological Sciences and Chemistry/Biochemistry, Arizona State University, Tempe Arizona 85287

Abstract

High-resolution transmission electron microscopy (HRTEM) affords a close look at the complex structures and intergrowths of the serpentine minerals. All contain alternating sheets of cations in tetrahedral and octahedral coordination. Lizardite, the flat species, forms in sufficiently large and well-ordered crystals to permit reliable X-ray structure determinations, and it is the reference mineral for estimates of the structures of antigorite and chrysotile. However, even lizardite forms in a wide variety of polytypes, only some of which have been explored. It also forms polygonal serpentine, a roughly cylindrical variety that typically consists of 15 or 30 sectors, each of which consists of lizardite layers. HRTEM images of the structure at sector boundaries show offsets of fringes that we interpret as the result of inversions of the tetrahedral sheets.

Using lizardite as the basis for an estimate of the curled chrysotile structure, we obtained atomic coordinates and used them to calculate fiber-axis X-ray and electron-diffraction patterns for polytypes. HRTEM images obtained viewing down the fiber axis show no ordering between layers. Chisholm (1988) reported 2*mm* symmetry for fibers when viewed perpendicular to their length, but most of our measured fibers show no symmetry for such orientations. Employing Fourier transforms of HRTEM images, we found a new one-layered orthorhombic chrysotile polytype with mirror symmetry perpendicular to the fiber axis.

Antigorite is notable for its conspicuous, modulated structure. We observed the waves to be asymmetrical and infer that the asymmetry results from an inhomogeneous distribution of hydrogen bonding between the layers. This distribution helps with a long-standing problem by explaining some apparently anomalous features of HRTEM images. The abundant (001) faults in antigorite are produced by boundaries of lamellae having different modulation profiles.

HRTEM images show the relations of serpentine minerals to each other as well as their host materials. Areas exist where layers of each of the serpentine minerals grade continuously and free of faults from one variety to another. The resulting intermediate or partial structures defy categorization into simple mineral types.

Introduction

THE MAGNESIAN SERPENTINE minerals are trioctahedral phyllosilicates with idealized composition $Mg_3[Si_2O_5(OH)_4]$. The most abundant minerals are antigorite, chrysotile, and lizardite. Although the Mg:Si ratio in antigorite is slightly smaller than in chrysotile and lizardite, antigorite is often grouped with the others because of the close genetic, crystal-chemical, and structural relationships of the three minerals. Serpentinite rocks, which have played a major role in the work of R. Coleman (e.g., Coleman, 1961, 1971a, 1971b), typically consist of mixtures of two or more of the serpentines.

Serpentine minerals are abundant as retrograde metamorphic alteration products of ultrabasic rocks and of the more magnesian minerals in other magmatic rocks, where they typically form through hydrothermal processes (Hess, 1933; Wenner and Taylor, 1974). They are also important carriers of water in subduction slabs (Ulmer and Trommsdorff, 1995; Bostock et al., 2002; Hyndman and Peacock, 2003), and they form aseismic regions within subduction slabs (Hyndman et al., 1997; Peacock and Hyndman, 1999). They are common components of altered primitive carbonaceous chondrite meteorites (Bunch and Chang, 1980; Barber, 1981; Tomeoka and Buseck, 1985, 1990; Buseck and Hua, 1993; Brearley, 1997). Bailey (1988) and Wicks and O'Hanley (1988) provided a comprehensive review of serpentine mineralogy, Chernosky et al. (1988) and Bromiley and Pawley (2003) summarized the results of experimental studies of the phase

[1]Permanent address: Department of Mineralogy, Eötvös Loránd University, H-1117 Pázmány P. sétány 1/C, Budapest, Hungary.

[2]Corresponding author; email: pbuseck@asu.edu

relations, and Evans (2004) reviewed serpentine occurrences and phase relations.

The serpentine minerals consist of octahedral (**O**) and tetrahedral (**T**) sheets that form **TO** (1:1) layers that are stacked to form various polytypes (Rucklidge and Zussman, 1965; Krstanovic, 1968; Mellini, 1982). In the absence of element substitutions such as Al for Si and Mg in lizardite, a misfit in dimensions between the **T** and **O** sheets is characteristic of the serpentine minerals. To accommodate the misfit, the minerals tend to assume curled or modulated structures in which the **T** sheets expand and the **O** sheets contract. The details of their structures can be complex and are best observed using high-resolution transmission electron microscopy (HRTEM).

In spite of extensive work, questions remain regarding the structures of the serpentine minerals. Many researchers have studied lizardite (Mellini, 1982; Mellini and Zanazzi, 1987; Mellini and Viti, 1994; Krstanovic and Karanovic, 1995; Brigatti et al., 1997; Guggenheim and Zhan, 1998; Zhukhlistov and Zvyagin, 1998), and its structure is the best known of the serpentine minerals. However, the details of its relation to polygonal (formerly called Povlen-type) serpentine are not well understood. Using electron microscopy, Dódony and Buseck (2004a) recognized a new lizardite polytype and inferred a new group of polytypes that still need to be detailed. X-ray crystal structure determinations of chrysotile do not exist, and its structure is based largely on indirect modeling experiments (Whittaker, 1953, 1955a, 1955b, 1956a, 1956b, 1956c). The original model of antigorite (Kunze, 1956, 1958, 1961), sometimes called a half-wave model, was refined using data from HRTEM images (Dódony et al., 2002) and single-crystal X-ray diffraction (Capitani and Mellini, 2004), but details such as possible polytypism and modulations remain unresolved.

Transmission electron microscopy has proven effective in providing detailed results about microstructures, textural and structural relationships, and thus greater insight into their growth and reaction mechanisms (Veblen and Buseck, 1979; Mellini et al., 1987; Viti and Mellini, 1998). Here we use the lizardite structure as a reference for the other serpentine minerals. Following a discussion of the structural features of lizardite, we provide examples of disordered stacking, coherent intergrowths of lizardite and chlorite, HRTEM images of polygonal serpentine, and HRTEM images and simulated diffraction data of chrysotile structures both along and perpendicular to the fiber axis.

Materials and Experiments

We studied serpentine samples from several geologic environments. The lizardite is a splintery variety labeled "baltimorite" that is intimately intergrown with chlorite. It occurs in a serpentinite that formed as an alteration product of olivine and pyroxene in dunites and gabbros (the Baltimore mafic complex, near the Maryland–Pennsylvania state border) from a marginal basin inland from a volcanic arc or a sub-arc plutonic complex (Hanan and Sinha, 1989). The polygonal serpentine is from a vein in a massive serpentinite near Jaklovce (Szepes-Gömör Mts., Slovak Republic). Both specimens are from the Collection of the Mineralogical Dept. of Eötvös University, Budapest, Hungary. The chrysotile samples are from Asbestos (Quebec, Canada), the Half Moon Bay area (California), and the Philips and Canadian Mines (Salt River Canyon, Arizona). The first two are from cross-fiber veins in massive serpentinites, and the others are metasomatic and formed along the contact between chert-bearing carbonates and diabase. The metasomatic samples consist of porcelainous, splintery, and asbestiform material. The splintery one seems to be transitional between the chert and long-fiber chrysotile. The antigorite samples are from Val Antigorio (Italy) and the Deligh quarry (Baltimore County, Maryland). The Val Antigorio sample is a foliated antigorite schist, and the other is from massive serpentinite.

Samples were prepared for TEM study through Ar-ion milling in order to obtain regions that permit viewing parallel to the serpentine layers. The thinned samples were lightly coated with carbon to avoid charging. Chrysotile fibers were crushed under ethanol and deposited onto copper grids covered by lacey-carbon supporting films to obtain fibers having their lengths perpendicular to the viewing direction. A JEOL 4000EX (400 kV; top-entry, double-tilt stage; c_s = 1 mm) transmission electron microscope was used for HRTEM imaging. Crystals were aligned along their main crystallographic directions, and selected-area electron-diffraction (SAED) patterns were recorded.

Fourier transforms were generated using Gatan Digital Micrograph 2.5.7 software (Meyer et al., 1996) to check experimental conditions such as crystallographic orientation, resolution, astigma-

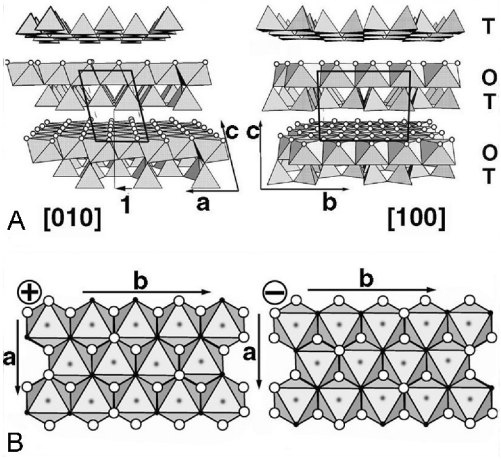

FIG. 1. Sketch of the lizardite structure. A. Perspective views along [010] (left) and [100] (right) of one-layer monoclinic lizardite. The projected unit cell is indicated by parallelograms. The tetrahedral and octahedral sheets are labeled **T** and **O**, respectively. The projection of the **c** axis on the **a**-**b** plane (arrow 1) indicates the **a**/3 displacement of adjacent **TO** layers. B. The **+** and – symbols indicate the slants of the octahedra in the **O** sheets. Small open circles indicate hydroxyl units.

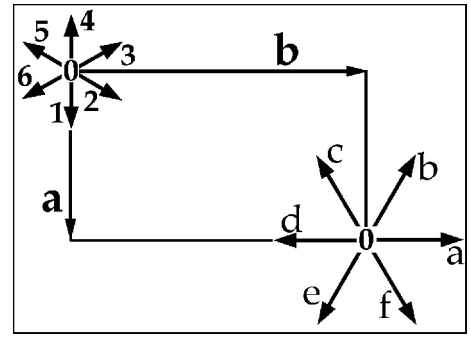

FIG. 2. Possible shift vectors between adjacent lizardite layers: shift vectors **1** to **6** are for <100> and shift vectors *a* to *f* are for <010>. Cases in which there is no shift are labeled 0.

tism, and to approximate diffraction information from small areas in HRTEM images. To reduce background noise, background subtraction was applied to selected digitized images using the same software. We simulated HRTEM images and SAED patterns from numerical structure data using a combination of the atomic positions of lizardite layers (Mellini, 1982) and Cerius^2 4.0 software (Molecular Simulation Institute, Inc.).

Lizardite

Lizardite is the most abundant serpentine mineral exposed in Earth's upper crust and is the basis for structure determinations of the other serpentines. The coupled substitution of M^{3+} for Mg and Si relieves the dimensional misfit, yielding a flat structure (Fig. 1) and the composition $(Mg_{3-x}M^{3+}_x)[Si_{2-x}M^{3+}_xO_5(OH)_4]$, where M^{3+} is commonly Al but can also be Fe or Cr (Caruso and Chernosky, 1979). The value of x lies between 0 and 0.5, with a usual value around 0.1.

Polytypism in **TO** phyllosilicates like lizardite is well established (Staedman and Nuttal, 1962, 1963, 1964; Rucklidge and Zussman, 1965; Jahanbagloo and Zoltai, 1968). Zvyagin et al. (1966) and Bailey (1969) derived lizardite polytypes on the assumption that **a**/3 and **b**/3 shifts of adjacent layers do not occur within the same crystal. Bailey and Banfield (1995) provided a comprehensive review of the polytype derivations, including those in which **a**/3 and **b**/3 shifts occur within the same crystal. The <100> and <110> directions are symmetrically equivalent in each lizardite layer, as are <010> and <310>. For displacements, we use the terms "**a**/3-type" and "**b**/3-type" to indicate shifts of 1/3[100] or 1/6[110] and 1/3[010] or 1/6[310], respectively.

The several polytypes differ in one or more of the following respects: (1) the relative slants of octahedra in adjacent layers, (2) the sequence of **a**/3-type shifts relating adjacent layers along [100] or [110], and (3) the sequence of **b**/3-type shifts along [010] or [310]. These conditions are illustrated in Figures 1 and 2, in which the orientation of octahedra are denoted as **+** or –. The identification of lizardite polytypes is based on their characteristic X-ray and electron-diffraction patterns (Zvyagin et al., 1966; Zvyagin, 1967; Bailey, 1969, 1988; Bailey and Banfield, 1995). Dódony (1997a) derived the possible two-layer lizardite polytypes and provided a method for their identification. Crystallographic data for these polytypes are listed in Table 1.

The results of X-ray structure refinements are consistent with the derivation of lizardite polytypes by Zvyagin et al. (1966), Bailey (1969), and Bailey and Banfield (1995). The stacking of successive **TO** layers was assumed to occur such that hydrogen bonding develops between each basal oxygen of a given **T** sheet and the outer hydroxyls of the **O** sheet in the adjacent layer. HRTEM is useful for studying polytypism, although the identification of polytypes

TABLE 1. Lizardite Polytypes Derived using data from Mellini (1982)[1]

Sequence of shift vectors and octahedral slants; Ramsdell symbol	**c** (Å)	α (º)	β (º)
0+, 1*T*	7.233	90	90
1+, 1*M*	7.45	90	76.19
a+, 3*R*	7.86	113.06	90
0+0–, $2H_1$	14.47	90	90
0+1+, $2M_3$	14.58	90	83
0+1–, $2M_4$	14.58	90	83
1–2+, $2M_2$	14.79	84.03	79.62
1+3+, $2M_1$	14.58	83.94	86.5
1–4+, 2*O*	14.47	90	90
a+a–, 6*R*	15.72	113.06	90
0+a+, $6R_3$	14.79	77.99	90
0+a–, $6R_2$	14.79	77.99	90
a+b+, 2*T*	15.42	72.57	99.96
a+b–, $2H_2$	15.42	72.57	99.96
a–2+, $4M_1$	15.21	72.33	86.65
a–2–, $4M_2$	15.21	72.33	86.65
4–1+, $2M_5$	**14.47**	**90**	**90**

[1]All have **a** = 5.332, **b** = 9.235 Å, and γ = 90º. The data for the non-H-bonded **4-1+** polytype are in bold.

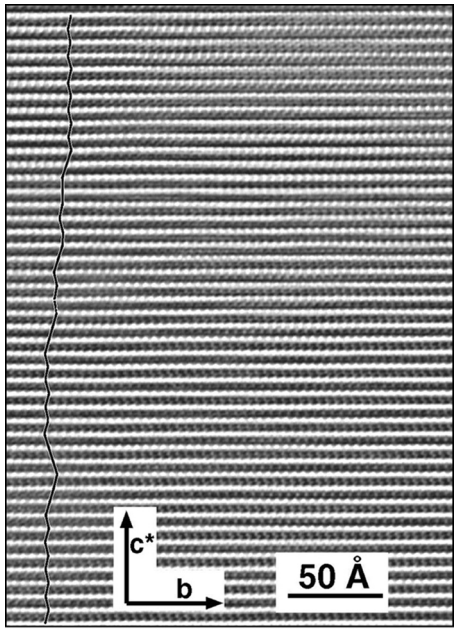

FIG. 3. <100> HRTEM image of random stacking in lizardite. The zigzag line shows the projection of the **c** axis between adjacent layers. (Baltimore mafic complex.)

using HRTEM requires two or more viewing directions parallel to the layers. No such paired images of lizardite have been published to date. However, single images can provide qualitative information about the stacking order.

Almost all lizardite grains in massive serpentinites show streaked SAED patterns, indicating that the stacking is commonly disordered. Figure 3 shows random stacking in a <100> projection, although locally ordered regions may exist (Fig. 4). The zigzag line indicates the projection of **c** vectors. Comparing HRTEM images to various structure models, we deduced the separations between oxygen atoms in the **T** sheets and those presumably bonded to H in the adjacent **O** sheets. On this basis, we identified a lizardite polytype with **4-1+** stacking and O—H distances out of the H-bonding range (Table 1) and inferred a new group of lizardite polytypes that is not H-bonded (Dódony and Buseck, 2004a).

Banfield and Bailey (1996) studied lizardite-chlorite interstratification, and Schmidt and Livi (1999) gave an example of the relation between polytypism and conditions of formation of chlorite in a metamorphic area. In the sample of baltimorite we

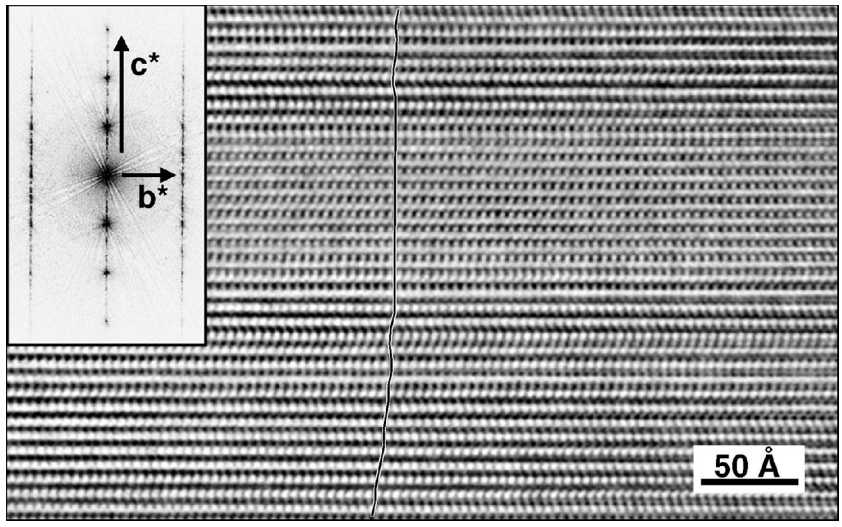

FIG. 4. <100> HRTEM image of an ordered region of lizardite hosted within a larger region with random stacking. The zigzag line shows the projection of the **c** axis between adjacent layers. A calculated diffractogram of the imaged area is inserted. No indications of order appear in the diffraction pattern. (Baltimore mafic complex.)

found that lizardite and chlorite layers can mix on the unit-cell scale via (001) interstratification (Fig. 5). Based on textural relations, Lapham (1958) suggested that chloritization in samples from the Baltimore complex postdated serpentinization.

Lizardite is the best-studied serpentine mineral, but a related less-understood form called polygonal serpentine also exists. It has a cylindrical shape and consists of radial sectors of lizardite (Cressey and Zussman, 1976; Mellini, 1986; Chisholm, 1992; Dódony, 1993; Baronnet et al., 1994; Cressey et al., 1994; Baronnet and Devouard, 1996; Baronnet and Belluso, 2002). We discuss polygonal serpentine together with lizardite because of the similarity of the two structures. However, polygonal serpentine, like chrysotile, has a fibrous morphology, and so some authors group those two materials together. The distinction, at least with the current state of knowledge, seems arbitrary.

Chisholm (1992) recognized that polygonal serpentine must contain either 15 or 30 sectors of lizardite-type material. Chisholm (1992) and Baronnet et al. (1994) presented models for both 15- and 30-sectored polygonal serpentine. However, Dódony (1997b) showed that there is a mismatch between experimental TEM results and these models. The model of Dódony for the 30-sectored polygonal serpentine matches experimental diffraction geometry and intensities as well as simulated TEM images.

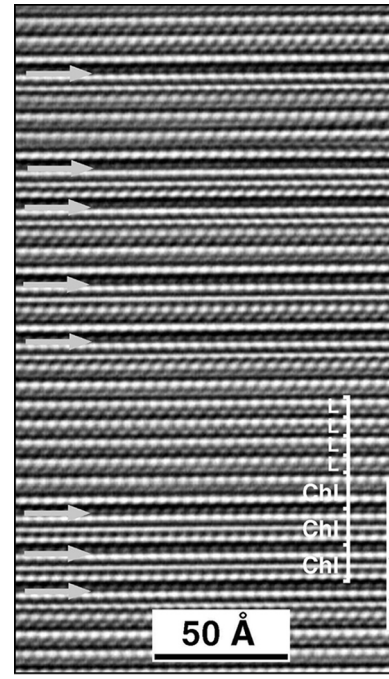

FIG. 5. <100> HRTEM image of lizardite-chlorite interstratification. Some chlorite (Chl) and lizardite (L) layers are indicated. The **T** sheets in an interstratified area are detailed on the right. The brucite-like sheets in the chlorite are indicated by arrows. (Baltimore mafic complex.)

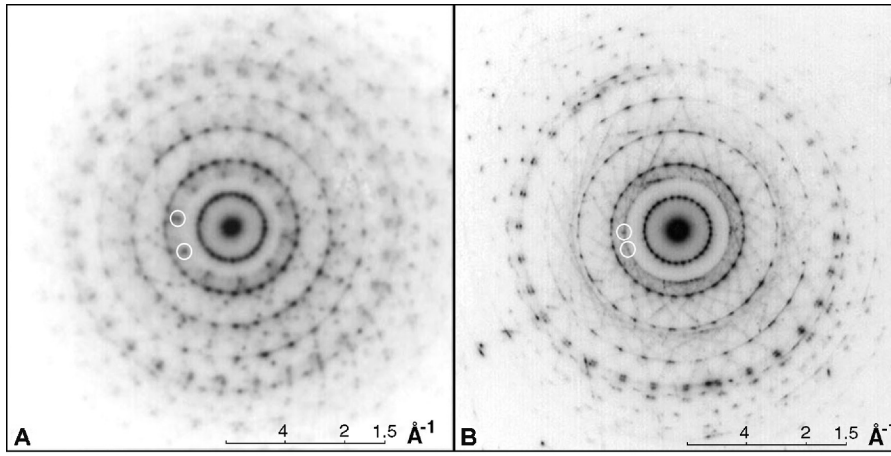

FIG. 6. SAED patterns of 30-sectored polygonal serpentine projected parallel to the fiber axis. A. The one-layered polytypes give rise to 10 020_{Liz} reflections (two are circled). B. The 20 020_{Liz} reflections (two are circled) indicate two-layered lizardite polytypes, but the non-uniform intensities show some disorder. The image of this grain is given in Figure 7. (Jaklovce.)

Because of the lack of appropriate diffraction data and high-resolution images, the 15-sectored polygonal serpentine is less understood than the 30-sectored one.

The SAED pattern in Figure 6A conforms to the structure model inferred for 30-sectored polygonal serpentine consisting of one-layered lizardite polytypes (Dódony, 1997b). However, faint reflections indicate disordered stacking. Figure 6B differs from Figure 6A in that the number (20) of 020 lizardite reflections is doubled, which indicates either two-layered or two different one-layered polytypes in each sector. The spacing of two-layered polytypes is visible in the central part of the polygonal serpentine (Fig. 7), but the outer ring differs in stacking in each sector. An enlarged area (Fig. 8) shows the offsets between adjacent sectors caused by inversions in the tetrahedral sheets.

Chrysotile

Chrysotile is the least abundant but commercially most significant of the Mg serpentine minerals. Because of its tubular structure and fibrous texture, it is also one of the most fascinating of all minerals. The lateral misfit between its **O** and **T** sheets is relaxed by continuous curling (Fig. 9), with the axis of curvature parallel to a [uv0] direction of what would be lizardite if the chrysotile were flattened. Whittaker (1953, 1955a, 1955b, 1956a, 1956b, 1956c) produced the first descriptions of the chrysotile structure. He based his results on X-ray measurements and analogue studies that utilized masks to simulate diffraction patterns that could then be compared to experimental data. He defined the chrysotile structures relative to reference lizardite (which has similar spacings along **a** and **b**) to explain the axes of curvature and polytypism. Devouard and Baronnet (1995) and Amelinckx et al. (1996) refined this approach for their improved descriptions of the chrysotile structure. Yada (1967, 1971, 1979) obtained HRTEM images of chrysotile, and confirmed the X-ray predictions about its cylindrical nature. Evans (2004) reviewed the energy considerations that influence and ultimately control its growth and radial dimensions.

Wicks and Whittaker (1975) revised the polytype nomenclature originally used by Whittaker. They noted the existence of a range of materials with chrysotile topology, all having a [100] fiber axis, but differing in the relative placements of the concentric single-layered tubes. Adjacent layers in chrysotile are displaced along the fiber axis, i.e., along **a** of reference lizardite, with values that differ from **a**/3 and have **+** or **-** slants for the octahedra. Data for the polytypes described by Wicks and Whittaker (1975) are presented in Table 2.

The above studies were done using analogue methods (a complete X-ray structure refinement of chrysotile does not exist). In contrast, the simula-

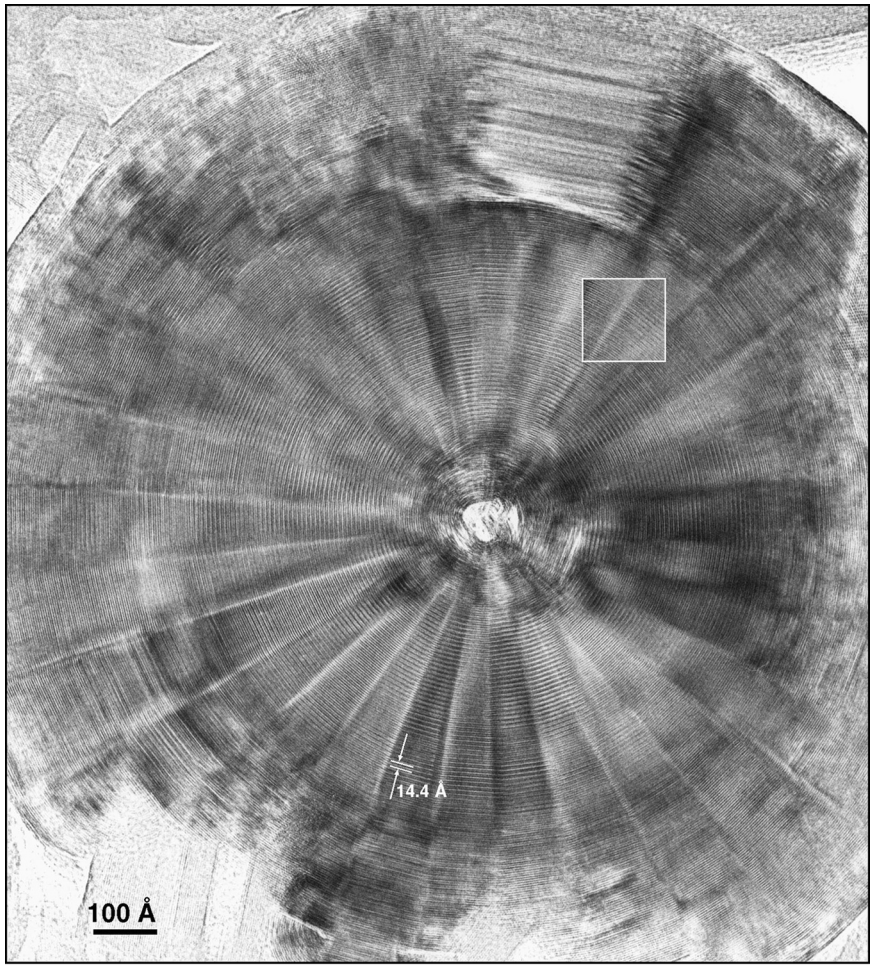

FIG. 7. TEM image of 30-sectored polygonal serpentine viewed down its fiber axis (its SAED pattern is in Fig. 6B). The inner part of the fiber consists of chrysotile (Chr) surrounded by a ring of sectors with two-layered lizardite polytypes (d_{001}=14.4 Å). The outermost zone of the fiber consists of disordered lizardite. The area in the white box is enlarged in Figure 8A. (Jaklovce.)

tions in this paper, as well as those by Dódony and Buseck (2004b), are based on atomic coordinates, and thus yield results that can be used for quantitative comparisons to observed data.

Fibrous minerals like chrysotile and polygonal serpentine are commonly studied by the fiber-axis X-ray diffraction method (Wicks and O'Hanley, 1988). Combining the results of Wicks and Whittaker (1975) with the atom coordinates determined by Mellini (1982) for lizardite, we estimated atom positions for chrysotile. We used these data to calculate fiber-axis patterns (for non-distorted reciprocal-lattice geometry) for the polytypes described by Wicks and Whittaker (1975) (Fig. 10).

The symmetry of chrysotile along the fiber axis has been controversial. Cressey and Whittaker (1993) agreed with the inferences of Whittaker (1955a) regarding the 5-fold symmetry of chrysotile projected down the fiber axes. Simulated SAED patterns for the four Wicks and Whittaker polytypes are identical to one another in fiber-axis projections (Fig. 11) and in good agreement with the results of Devouard and Baronnet (1995). However, our experimental data contradict these theoretical results in

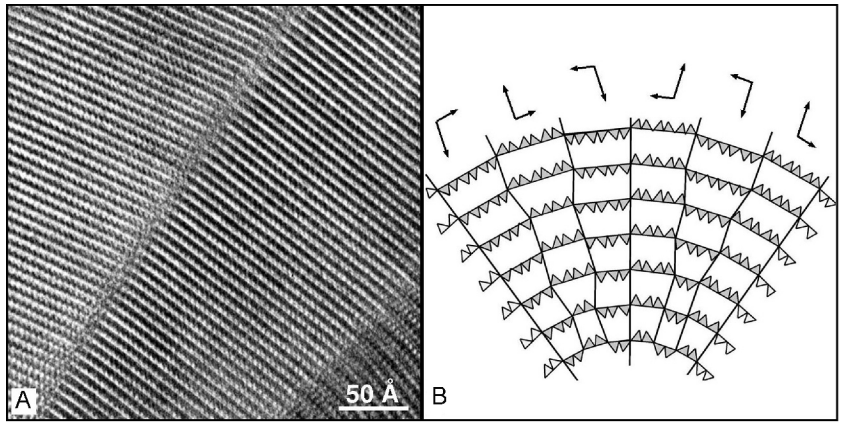

FIG. 8. A. Enlarged area indicated in Figure 7 showing offsets of lizardite layers at sector boundaries. B. Schematic sketch of the **T** sheets in a 30-sectored polygonal serpentine. Inversions occur in the **T** sheets at sector boundaries. The polytypes in adjacent sectors are indicated by their **b** and **c** axes. The diagonal interface in (A) corresponds to one of the sector boundaries in (B). (Jaklovce.)

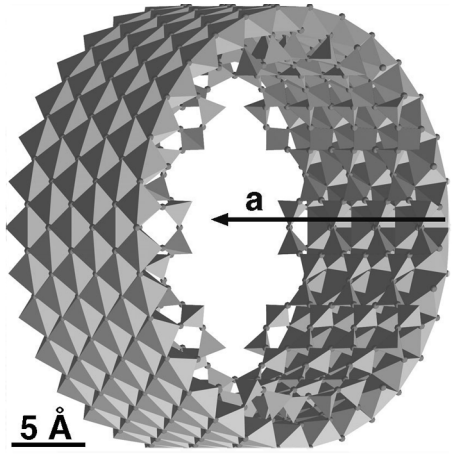

FIG. 9. Perspective view of a cylindrical chrysotile layer. The **O** sheet surrounds the **T** sheet. The fiber axis is parallel to the **a** axis of the reference lizardite structure.

that our HRTEM images show neither 5- nor 10-fold symmetry.

Figure 12 shows a HRTEM image and corresponding Fourier transform of chrysotile viewed down its fiber axis. The figure shows continuous intensities even in the second ring (representing the **b**/2 spacing of reference lizardite), in which one would not normally expect streaking unless there was random stacking. In contrast, the SAED pattern predicted for chrysotile polytypes in Figure 11 shows 10 distinct spots. Most chrysotile samples that we have observed contain such continuous 020_{Liz} bands, which indicate random rotations of adjacent layers.

The polytypes were originally defined by their displacements along the fiber axis (parallel to **a**) but without constraints along the **b** direction. We adopt that convention, although there clearly are difficulties because, for example, it gives rise to situations in which apparently random rotations of adjacent layers are compatible with the lack of randomness implied by polytypes.

Chisholm (1988) predicted 2*mm* symmetry of chrysotile patterns when viewed perpendicular to the fiber axis. He also reported that SAED patterns should have the same symmetry as ones obtained by fiber-axis X-ray diffraction. However, we observe no symmetry in most HRTEM images having this orientation (Fig. 13). In contrast, the image in Figure 14 and its Fourier transform (Fig. 14B) indicate orthorhombic symmetry, with a spacing different from that of the $2Or_{c1}$ polytype defined by Wicks and Whittaker and shown in Table 2. This is an example of a new chrysotile polytype. The details of chrysotile structures, their calculated X-ray fiber-axis patterns, and simulated SAED patterns are discussed by Dódony and Buseck (2004b).

Antigorite

Antigorite occurs in mafic and ultramafic rocks of uppermost prehnite-pumpellyite to amphibolite facies of regional metamorphism as well as in some carbonate rocks in regional- and contact-metamor-

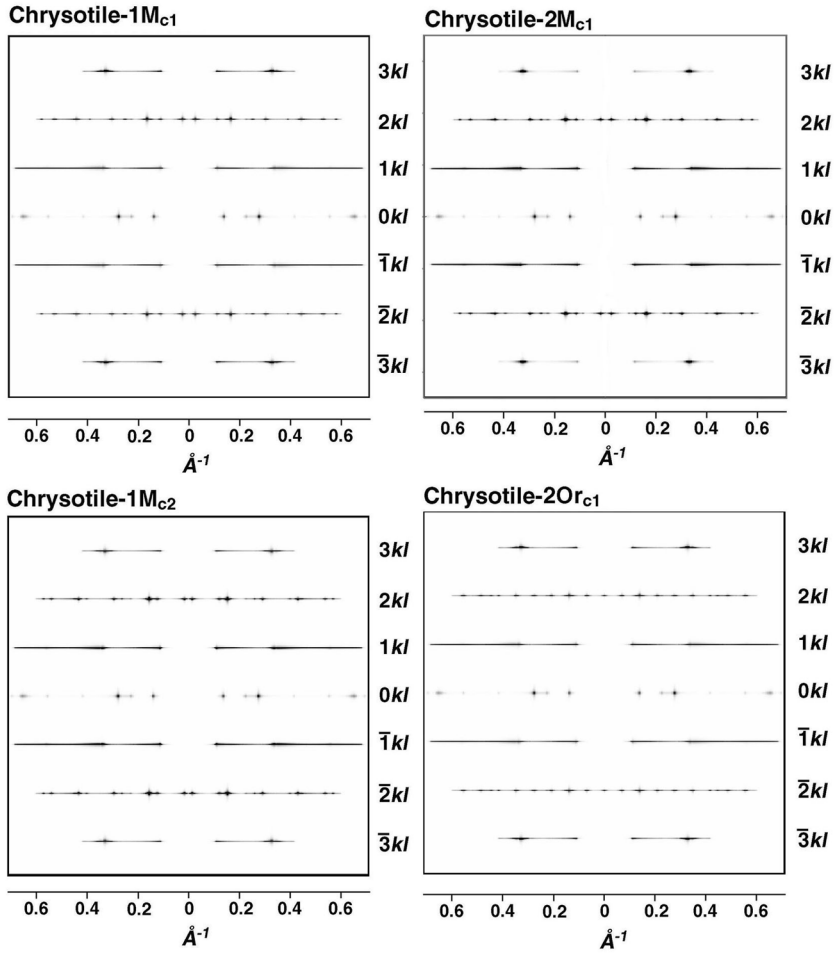

FIG. 10. Calculated fiber-axis X-ray diffraction patterns of chrysotile polytypes (Wicks and Whittaker, 1975) using atomic positions for fibers with 323-Å diameter. The indices refer to the reciprocal-lattice planes of the reference lizardite structure.

TABLE 2. Chrysotile Polytypes of Wicks and Whittaker (1975)[1]

Polytype	[100] shift sequence [in Å]	Slant sequences of octahedra	β (°)
$1M_{c1}$	… 0.5 …	…+…or …– …	94.1
$1M_{c2}$	… 0.3 …	…+…or …– …	92.5
2Mc1	… 0.5, 03 …	…+…or …– …	93.3
$2Or_{c1}$	…0.5, –0.5…or …0.3, –0.3…	…+ –…	90

[1]The shifts between adjacent layers are in the opposite direction from the shifts used by Zvyagin et al. (1966) and Bailey (1969) for lizardite polytypes.

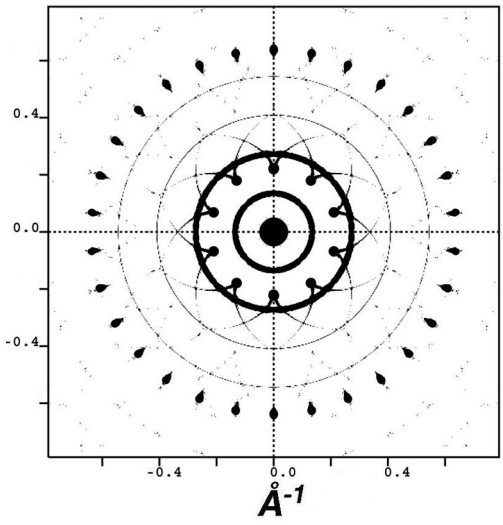

FIG. 11. Simulated SAED pattern of chrysotile viewed parallel to the fiber axis based on atomic positions for a fiber with 323-Å diameter.

phic terranes (O'Hanley, 1996; Trommsdorff and Connolly, 1996). It is stable to depths of 90 to 150 km (Schmidt and Poli, 1998), is among the most hydrous rock-forming silicates, and is proposed to be the dominant phase for carrying water into the upper mantle during subduction of ultrabasic rocks (Ulmer and Trommsdorff, 1995; Peacock, 2001; Wunder et al., 2001).

Antigorite and lizardite differ both in composition and in structure, with antigorite having a distinctive wavelike structure parallel to **a** of the reference lizardite structure (Fig. 15). The Mg and OH contents decrease slightly in regions near the inversions of the corrugated **T** and O sheets. The composition can be expressed as $Mg_{3m-3}[Si_{2m}O_{5m}(OH)_{4m-6}]$, where m is the number of tetrahedral positions in a unit cell as seen in [010] projections.

In a TEM study, Mellini et al. (1987) observed an inverse proportionality between metamorphic grade and the m-values of antigorite. However, they pointed out the limited applicability to geothermometry because most antigorite shows a heterogeneous distribution of m-values even within individual crystals. Wunder et al. (2001) showed a close connection between the m-value, temperature, and pressure.

Our structure model was derived from HRTEM and SAED measurements (Dódony et al., 2002), retaining the original half-wave configuration proposed by Kunze (1956) but without his four- and eight-membered silicate rings at every second inversion along **a**. Our HRTEM images show no traces of such rings (Fig. 16), although even recent papers (Auzende et al., 2002; Grobéty, 2003) utilize the Kunze model.

Another discrepancy exists between experimental TEM images and images calculated using the standard Kunze (1956) half-wave model for antigorite. The calculations predict that all (200) fringes in [010] HRTEM images are of equal intensity. However, experimental images show differences, with alternate (200) fringes everywhere being weaker. Spinnler (1985) suggested that the dark

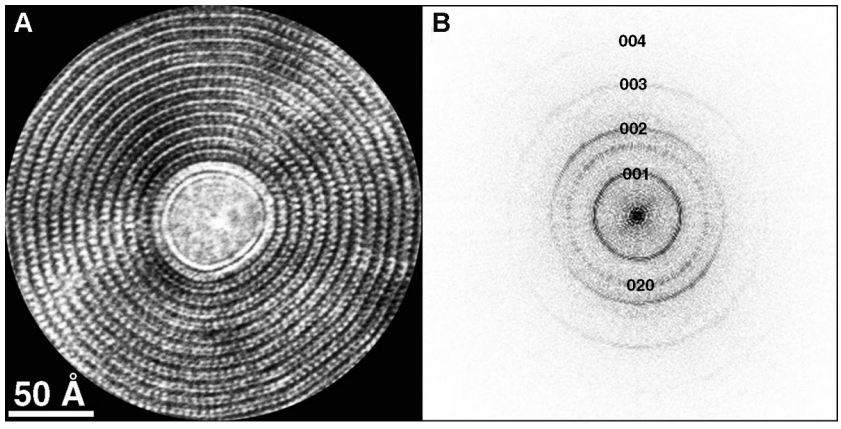

FIG. 12. A. HRTEM image of a chrysotile fiber viewed down the fiber axis. B. Fourier transform of the image in (A). The indices refer to the reference lizardite structure. The continuous 020 ring indicates disordered layer stacking. (Baltimore mafic complex.)

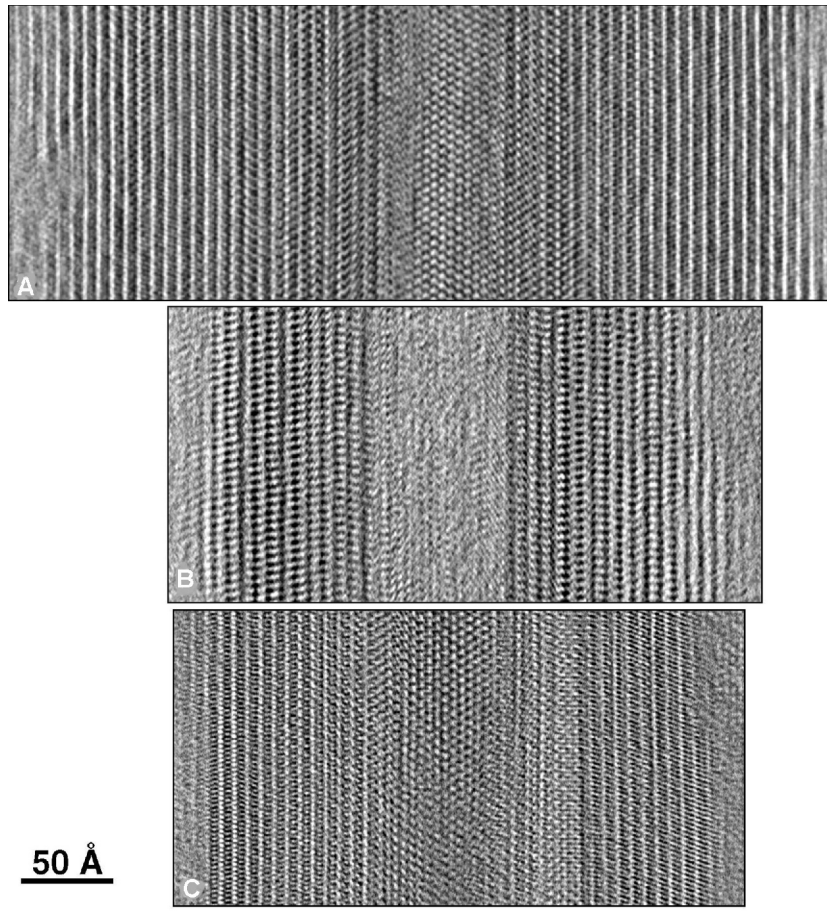

FIG. 13. HRTEM images of three chrysotile fibers projected perpendicular to the their lengths. The fiber cores are aligned with one another and are vertical in the figure. The appearances of both the cores and walls of the three fibers differ. The images show no symmetry. A. Asbestos. B. Half Moon Bay area. C. Canadian Mine.

fringes occur at the locations of the presumed eight-membered rings, where the T sheets reverse orientation. Otten (1993), on the other hand, concluded that alternate (200) fringes [he called them the "conspicuous (100) fringe(s)"] are in the positions of the reversals containing the six-membered rings of tetrahedra. The model of Dódony et al. (2002) provides compatible experimental and calculated results. Using that model, we interpret the above discrepancy as the result of a lack of eight-membered rings and an asymmetry on either side of the modulation wave. The modulation wavelength is evident in the images, as is the different contrast of alternating (200) fringes (Fig. 17).

The atomic positions for our antigorite model were used to produce the representation in Figure 18A, which we subsequently confirmed using the atomic positions determined by X-ray diffraction data of Capitani and Mellini (2004; Fig. 18B). We estimated the distances between the oxygen positions in the basal planes of **T** sheets and the (OH) planes of **O** sheets in adjacent antigorite layers and used the results to determine the extent to which H bonding occurs. H-bonded oxygens are closer to each other than non-bonded ones, and the strength of the bonds increases with their proximity (Brown, 1976, 1978; Ceccarelli et al., 1981). The model shows that the H—O separations between the **T** and

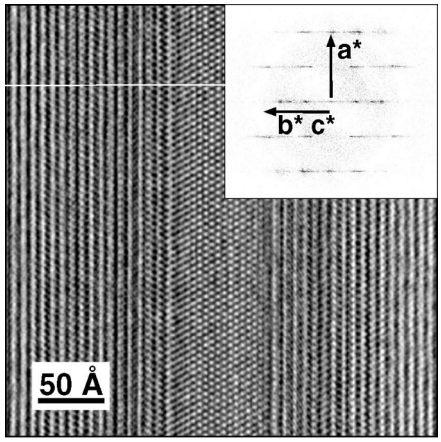

FIG. 14. HRTEM image of a chrysotile fiber projected perpendicular to its length. The fiber displays mirror symmetry, with a reflection plane indicated by a horizontal white line. The right and left sides of the image have different contrast, and no symmetry is evident parallel to the fiber axis. The inset depicts a Fourier-transform of the image. Intensities indicate orthorhombic symmetry. The 20*l* reflections indicate the one-layered character of this chrysotile. (Asbestos.)

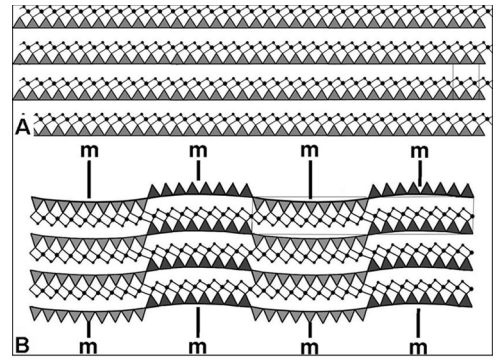

FIG. 15. Sketch of the lizardite and antigorite structures. A. [010] projection of lizardite, the reference structure for antigorite. B. [010] projection of antigorite (m = 17). The mismatch between **T** and **O** sheets is accommodated by bending of the structure. Each half of the antigorite wave shows mirror symmetry for the **T** sheets.

O sheets are less than 2.3 Å. We interpret these shorter separations as indicating the probable places of H bonding. These places are indicated by the short black lines that extend between adjacent **TO** layers (Fig. 18).

Hydrogen bonding provides stronger attractions between adjacent sheets in the regions near the cell origin than in the centers of the cells (Fig. 18). A consequence is that the separation of the layers is greater in the cell centers than around the origins. A further consequence is that the modulation profile differs from that proposed in the Kunze (1956) model, because each of the half-wave portions are distorted so that they no longer display mirror symmetry (Fig. 19). The more strongly H-bonded portions of modulation waves are brighter in the HRTEM images around the origin of the unit cells in the models of Dódony et al. (2002), indicating the unique character of alternate (200) planes. Although TEM studies have significantly improved our knowledge of antigorite, a mathematical description of the wave profile and polytypism of antigorite await more

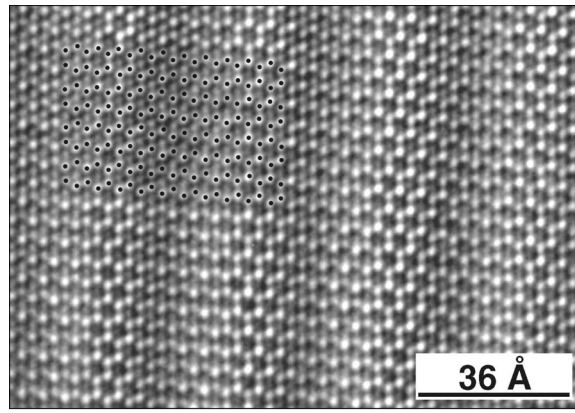

FIG. 16. [001] HRTEM image of an antigorite crystal with m = 14. The small black dots indicate the silicon positions; the **T** sheet is a continuous network of six-membered silicate rings. (Val Antigorio.)

precise measurements and more quantitative interpretations.

Our antigorite model, based on HRTEM data, lacks four- and eight-membered silicate rings. In contrast, the structure proposed by Capitani and Mellini (2004) based on single-crystal XRD measurements, does contain them. They propose that the difference may depend on whether m is even or odd. However, models based on our SAED and HRTEM data for m = 14 and 17 are free of such rings (Figs. 14 and 15, respectively, in Dódony et al., 2002). This apparent discrepancy between XRD and TEM results remains to be resolved.

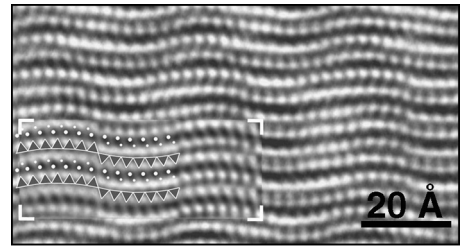

FIG. 17. [010] HRTEM image of an antigorite with m = 14. Calculated HRTEM image and the structural model are inserted in the area marked by white corners. The octahedral and hydroxyl positions are indicated be large and small white dots, respectively. (Val Antigorio.)

Textures and Transitions of Serpentines in HRTEM Images

The textural and structural relations among the serpentine minerals can be complex, and provide information about reactions that are not evident during study of the phases in isolation or at low magnifications. Furthermore, in a manner analogous to petrographic microscopy, TEM of serpentine textures can help reconstruct the history of mineral formation.

The fibrous morphology of chrysotile makes it intriguing. Depending on the geologic environment, it may form in several ways (Evans, 2004). Here, as an example, we discuss chrysotile formed during contact metasomatism of a carbonate-chert sequence intruded by a diabase sill. Figure 20 shows undamaged cross-sections of fibers in what appears to be an amorphous matrix that we believe to have been chert. Their subparallel orientation is consistent with growth in a diffusion gradient at a metasomatic contact (B. W. Evans, pers. commun., January 2004). The central cavities of these chrysotiles have roughly uniform diameters and appear to be empty.

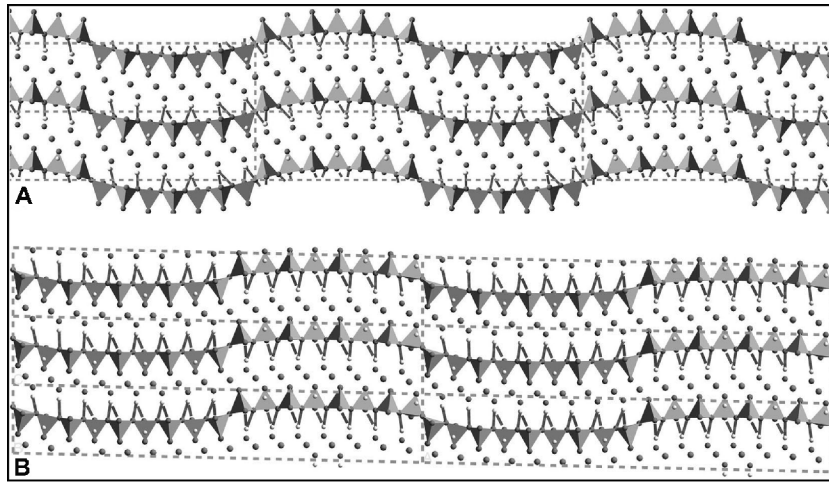

FIG. 18. Sketch of hydrogen bonds, shown by the thin black lines, in antigorite structures with (a) m = 14 (Dódony et al., 2002) and (b) m = 17 (calculated using data of Capitani and Mellini, 2004). The number of H bonds is greater near the cell origin (A) and cell center (B). Those bonds are drawn where the separation between oxygen in the **T** sheets and hydrogen in the **O** sheets is less than 2.3 Å. The cell origins for m = 14 and m = 17 antigorite are those of the source publications and are shifted by half a cell along **a.**

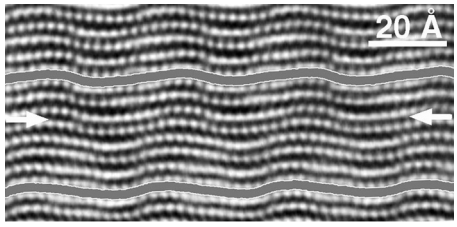

FIG. 19. [010] HRTEM image of an antigorite with m =14. A stacking fault is marked by arrowheads and separates regions having waves (bold bands) with opposite asymmetry as well as opposite slants in the **O** sheets. (Deligh quarry.)

There appears to be an inverse correlation between sizes of the central cavities and the number of surrounding layers of chrysotile (Fig. 21). Only a few poorly ordered chrysotile layers with low contrast and no traces of regular spacings occur around the largest holes. The holes are smaller within larger and better-ordered chrysotile grains. This puzzling relationship seems to suggest that the cavities preceded serpentine formation or perhaps formed simultaneously with incipient chrysotile formation. The interlayer spacings in these cases are irregular and suggest poor ordering. Figure 22, which shows

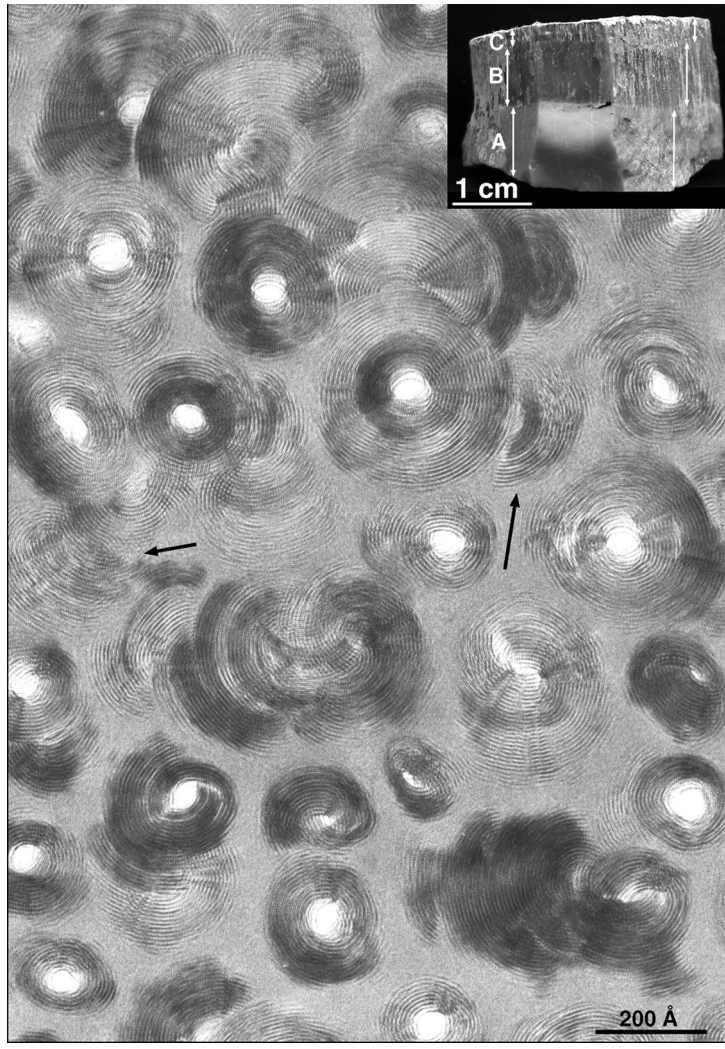

FIG. 20. HRTEM image of cross-sectioned irregular chrysotile fibers in an amorphous matrix that was presumably chert (layer B in the inset). The fiber cores appear to be empty, and the fibers are oriented subparallel to one another. Some incomplete fibers are marked by arrows. The inset shows (A) porcelainous, (B) splintery, and (C) fibrous materials. (Philips Mine.)

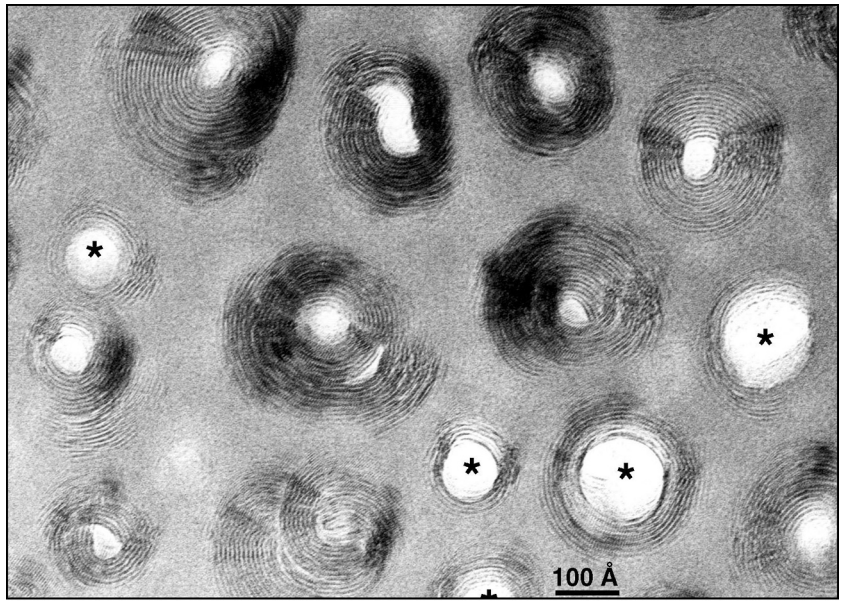

FIG. 21. HRTEM image of large holes (marked by stars) in an amorphous matrix surrounded by only relatively few chrysotile layers. (Philips Mine.)

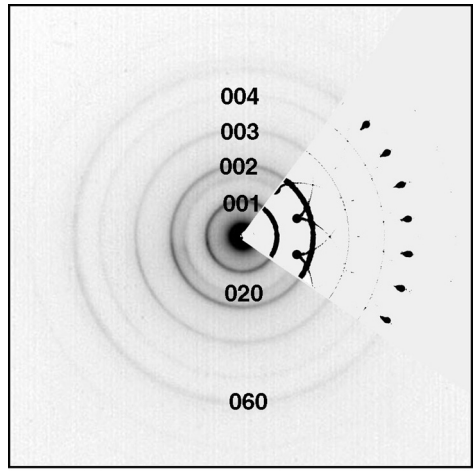

FIG. 22. SAED pattern of the area in Figure 21. The pattern is similar to a powder pattern, with the reflections forming rings. The spacings match those in the calculated SAED pattern in Figure 11, a portion of which is inserted on the right side. (Philips Mine.)

the 0kl spacings of chrysotile, is an SAED pattern of the area in Figure 21.

There are also partly curled layers without hollow cores in regions containing well-defined chrysotile fibers (arrows in Figs. 20 and 23). Some, like the arrowed example in Figure 23, appear to have one part crossing the other, suggesting ribbons with spiral structures.

Figure 24 shows an intergrowth of chrysotile, lizardite, and chlorite. The HRTEM image and

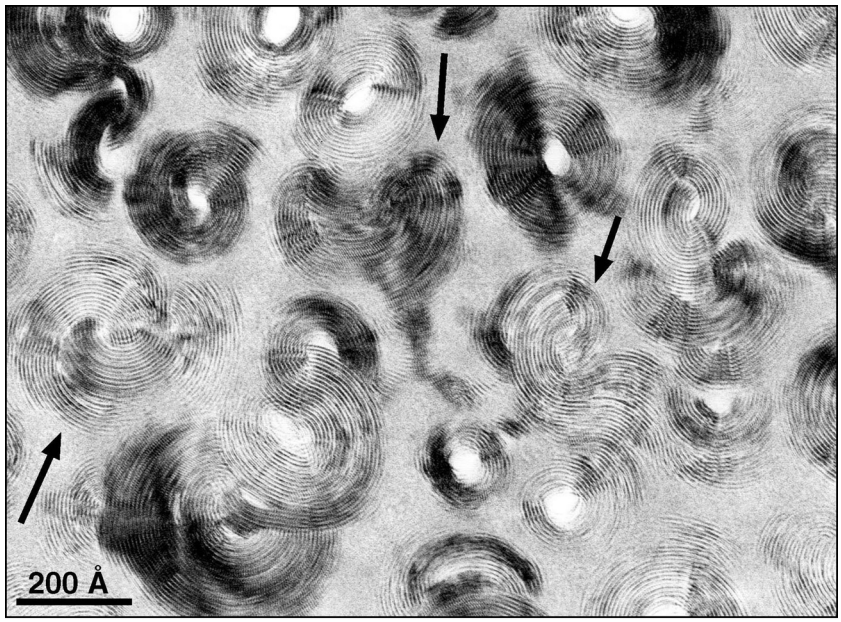

FIG. 23. HRTEM image of an area consisting largely of chrysotile-like grains, many of which are free of central cores (marked by arrows). Some appear to consist of curved ribbons. (Philips Mine.)

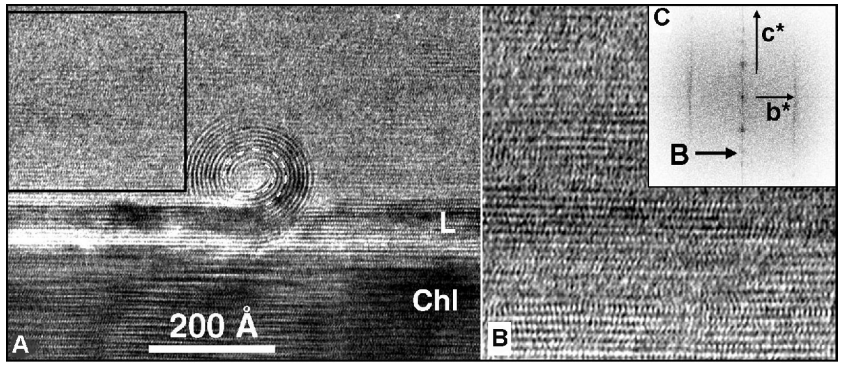

FIG. 24. A. HRTEM image of chlorite (Chl), lizardite (L), and a chrysotile fiber in partly ordered matrix (top). The lizardite forms a thin layer between the matrix and chlorite. The lizardite layers split into at least two ribbons, with one ribbon curled to form the chrysotile fiber. The weak horizontal fringes crossing the chrysotile fiber indicate that it is thinner than the sample. B. Enlarged and background-filtered image of the boxed area in (A), which contains 7.3-Å fringes of lizardite. C. Fourier transform of boxed area in (A). The pattern is consistent with disordered lizardite viewed along [100], but an additional pair of peaks (arrowed at B and explained in the text) occurs at 4.5±0.3 $Å^{-1}$. (Philips Mine.)

calculated diffraction pattern for the upper part of the figure suggest lizardite oriented parallel to $[100]_{Chl}$. The indicated area in Figure 24A is enlarged and background filtered in Figure 24B, with the calculated diffraction pattern inserted. Intensities indicate disordered stacking in a lizardite-like structure, and the intense continuous scattering provides evidence of an amorphous component. The faint, slightly diffuse intensity maxima (marked by B) have a spacing between 4.3 and

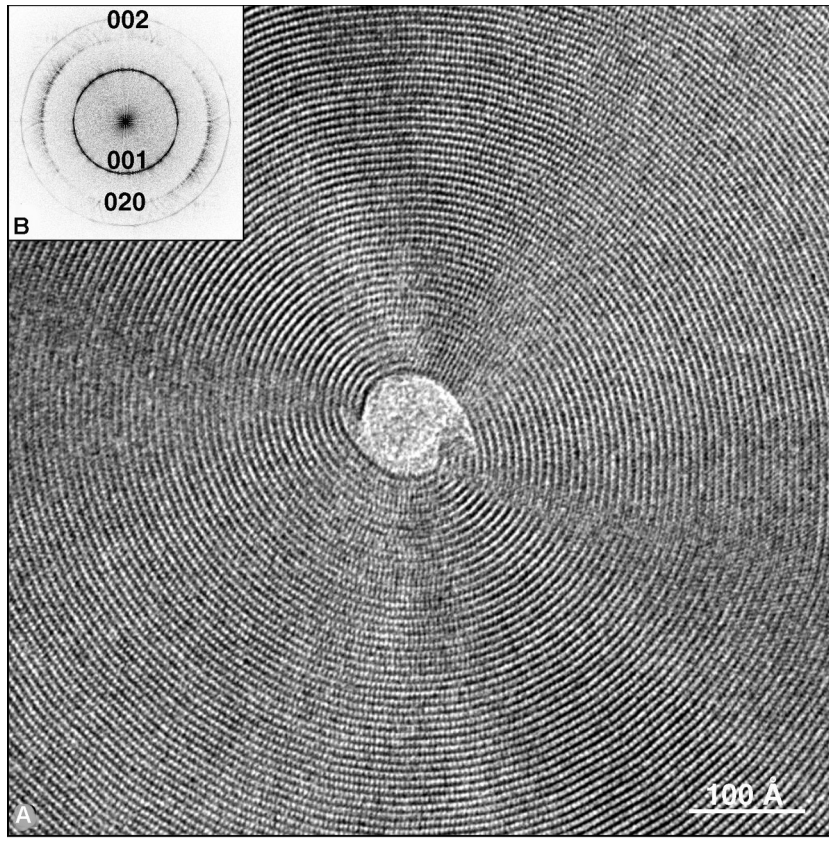

FIG. 25. A. HRTEM image down the fiber axis of a chrysotile fiber with a core that suggests a doubly coiled structure. It consists of three and five layers, respectively. B The Fourier transform of the HRTEM image indicates a lack of stacking order. (Jaklovce.)

4.7 Å. Based on this spacing and the composition of the matrix, we interpret this peak as indicating the presence of disordered brucite- and tetrahedral sheets in the matrix. The crystallinity of the surrounding matrix increases with proximity to the lizardite (L). No faults intervene between regions of chrysotile and lizardite in Figure 24A; therefore, we conclude that both must exhibit the same shift vectors in the direction of the projection, i.e., chrysotile has the same shift as lizardite along the **a** axis.

Only small quantities of chrysotile formed together with lizardite in this matrix. Figure 24A demonstrates that lizardite curls into chrysotile. Veblen and Buseck (1979), Buseck (1984), Buseck and Veblen (1988), Sharp et al. (1990), and Dódony (1993) have reported similar types of intergrowths and transitions, all of which raise questions about the discreteness of these minerals and about serpentine nomenclature.

An intriguing feature of chrysotile is the range of arrangements of layers within a fiber. In addition to concentric and scrolled layers (Yada, 1967, 1971; Baronnet and Belluso, 2002), there are bundles in which it appears as if groups of layers nucleated on opposite sides of what are now the cores (Fig. 25). It does not appear as if they grew by the familiar layer-by-layer or screw-dislocation mechanisms typical of sheet silicates. The HRTEM image shows a large chrysotile grain viewed along its fiber axis. It consists of two stacks of layers originating at the opposite sides of the fiber core. These stacks contain three and five layers, respectively, and one might expect the result of the growth of such material to result in an eight-layered periodicity. However, the

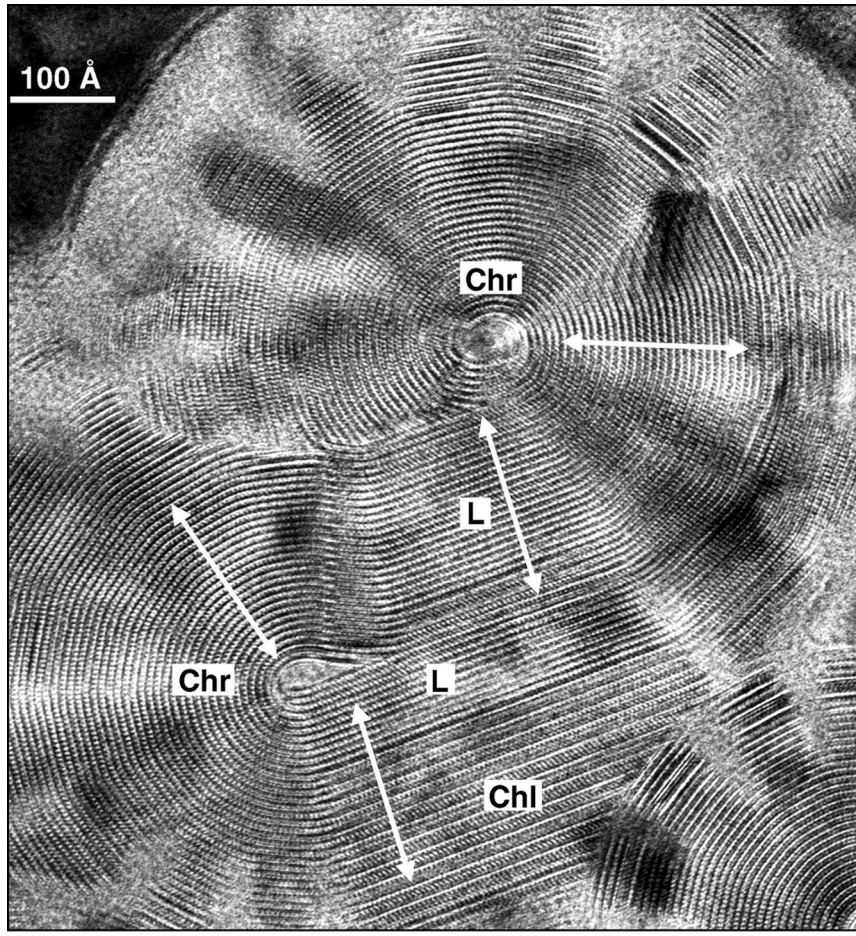

FIG. 26. HRTEM image of an intimate intergrowth of regions of chlorite (Chl), lizardite (L), and chrysotile (Chr). Each of these structures shows coherent, continuous boundaries with the others. See text for an explanation of the arrows. (Baltimore mafic complex.)

Fourier transform of this image consists of only the concentric rings of the corresponding lizardite 001, 020, and 002 reflections. There is no indication of ordering or an eight-layered periodicity in this projection.

Figure 26 shows an intimate intergrowth of material that, over short distances, could be considered to be lizardite (L), chrysotile (Chr) with its outer parts partly polygonized, and chlorite (Chl). The white arrows are all of the same length and indicate a continuous packet of material that is apparently folded back upon itself. The transitions are smooth, free of distortions, and discontinuities. Even the chlorite-chrysotile interface shows no strain contrast or break in continuity of the fringes. Phase definition is clearly an issue in a sample such as this.

Conclusions

The serpentine minerals display a rich range of structures and textures. They form in large quantities in geophysically significant regions. Gradational structures raise serious questions about phase definitions, and they remain fertile minerals for continuing research.

Acknowledgments

Electron microscopy was performed at the Center for High Resolution Electron Microscopy at Arizona State University. We thank David Bell, Bertrand Devouard, Bernard Evans, and Marcello Mellini for helpful reviews and comments; NSF grant EAR-0003533 provided financial support.

REFERENCES

Amelinckx, S., Devouard, B., and Baronnet, A., 1996, Geometrical aspects of the diffraction space of serpentine rolled microstructures: Their study by means of electron diffraction and microscopy: Acta Crystallographica, Section A, v. 52, p. 850–878.

Auzende, A. L., Devouard, B., Guillot, S., Daniel, I., Baronnet, A., and Lardeaux, J. M., 2002, Serpentinites from Central Cuba: Petrology and HRTEM study: European Journal of Mineralogy, v. 14, p. 905–914.

Bailey, S. W., 1969, Polytypism of trioctahedral 1:1 layer silicates: Clays and Clay Minerals, v. 17, p. 355–371.

_____, 1988, Polytypism of 1:1 layer silicates, *in* Bailey, S. W., ed., Hydrous phyllosilicates (exclusive of micas): Washington, DC, Mineralogical Society of America, Reviews in Mineralogy 19, p. 9–27.

Bailey, S. W., and Banfield, J. F., 1995, Derivation and identification of nonstandard serpentine polytypes: American Mineralogist, v. 80, p. 1104–1115.

Banfield, J. F., and Bailey, S. W., 1996, Formation of regularly interstratified serpentine-chlorite minerals by tetrahedral inversion in long-period serpentine polytypes: American Mineralogist, v. 81, p. 79–91.

Barber, D. J., 1981, Matrix phyllosilicates and associated minerals in C2M carbonaceous chondrites: Geochimica et Cosmochimica Acta, v. 45, p. 945–970.

Baronnet, A., and Belluso, E., 2002, Microstructures of the silicates: Key information about mineral reactions and a link with the Earth and materials sciences: Mineralogical Magazine, v. 66, p. 709–732.

Baronnet, A., and Devouard, B., 1996, Topology and crystal growth of natural chrysotile and polygonal serpentine: Journal of Crystal Growth, v. 166, p. 952–960.

Baronnet, A., Mellini, M., and Devouard, B., 1994, Sectors in polygonal serpentine — a model based on dislocations: Physics and Chemistry of Minerals, v. 21, p. 330–343.

Bostock, M. G., Hyndman, R. D., Rondenay, S., and Peacock, S. M., 2002, An inverted continental Moho and serpentinization of the forearc mantle: Nature, v. 417, p. 536–538.

Brearley, A. J., 1997, Phyllosilicates in the matrix of the unique carbonaceous chondrite Lewis Cliff 85332 and possible implications for the aqueous alteration of CI chondrites: Meteoritics and Planetary Science, v. 32, p. 377–388.

Brigatti, M. F., Galli, E., Medici, L., and Poppi, L., 1997, Crystal structure refinement of aluminian lizardite-$2H_2$: American Mineralogist, v. 82, p. 931–935.

Bromiley, G. D., and Pawley, A. R., 2003, The stability of antigorite in the systems MgO-SiO_2-H_2O (MSH) and MgO-Al_2O_3-SiO_2-H_2O (MASH): The effects of Al^{3+} substitution on high-pressure stability: American Mineralogist, v. 88, p. 99–108.

Brown, I. D., 1976, Geometry of O-H...O hydrogen bonds: Acta Crystallographica Section A, v. 32, p. 24–31.

_____, 1978, Bond valences—simple structural model for inorganic chemistry: Chemical Society Reviews, v. 7, p. 359–376.

Bunch, T. E., and Chang, S., 1980, Carbonaceous chondrites. 2. Carbonaceous chondrite phyllosilicates and light-element geochemistry as indicators of parent body processes and surface conditions: Geochimica et Cosmochimica Acta, v. 44, p. 1543–1577.

Buseck, P. R., 1984, Imaging of minerals with the TEM: Electron Microscopy Society of America Bulletin, v. 14, p. 47–53.

Buseck, P. R., and Hua, X., 1993, Matrices of carbonaceous chondrite meteorites: Annual Review of Earth and Planetary Sciences, v. 21, p. 255–305.

Buseck, P. R., and Veblen, D., 1988, Mineralogy, *in* Buseck, P. R., Cowley, J. M., and Eyring, L., eds., High-resolution transmission electron microscopy: New York, NY, Oxford University Press, p. 308–377.

Capitani, G., and Mellini, M., 2004, The modulated crystal structure of antigorite: The m = 17 polysome: American Mineralogist, v. 89, p. 147–159.

Caruso, L. J., and Chernosky, J. V., Jr., 1979, The stability of lizardite: Canadian Mineralogist, v. 17, p. 757–770.

Ceccarelli, C., Jeffrey, G. A., and Taylor, R., 1981, A survey of O-H ... O hydrogen-bond geometries determined by neutron-diffraction: Journal of Molecular Structure, v. 70, p. 255–271.

Chernosky, J. V., Berman, R. G., Jr., and Bryndzia, L. T., 1988, Stability, phase relations, and thermodynamic properties of chlorite and serpentine group minerals, *in* Bailey, S. W., ed., Hydrous phyllosilicates (exclusive of micas): Washington, DC, Mineralogical Society of America, Reviews in Mineralogy 19, p. 295–346.

Chisholm, J. E., 1988, Electron-diffraction patterns of chrysotile—effect of specimen orientation: Acta Crystallographica, Section A, v. 44, p. 70–75.

_____, 1992, The number of sectors in polygonal serpentine: Canadian Mineralogist, v. 30, p. 355–365.

Coleman, R. G., 1961, Jadeite deposits of the Clear Creek area, New Idria District, San Benito County, California: Journal of Petrology, v. 2, p. 209–247.

_____, 1971a, Petrologic and geophysical nature of serpentinites: Geological Society of America Bulletin, v. 82, p. 897–918.

_____, 1971b, Plate tectonic emplacement of upper mantle peridotites along continental edges: Journal of Geophysical Research, v. 76, p. 1212–1222.

Cressey, B. A., and Whittaker, E. J. W., 1993, 5-fold symmetry in chrysotile asbestos revealed by transmission electron microscopy: Mineralogical Magazine, v. 57, p. 729–732.

Cressey, B. A., and Zussman, J., 1976, Electron microscopic studies of serpentinites: Canadian Mineralogist, v. 14, p. 307–313.

Cressey, B. A., Cressey, G., and Cernik, R. J., 1994, Structural variations in chrysotile asbestos fibers revealed by synchrotron X-ray diffraction and high-resolution transmission electron-microscopy: Canadian Mineralogist, v. 32, p. 257–270.

Devouard, B., and Baronnet, A., 1995, Axial diffraction of curved lattices—geometrical and numerical modeling. Application to chrysotile: European Journal of Mineralogy, v. 7, p. 835–846.

Dódony, I., 1993, Microstructures in serpentinites: Microscopia Elettronica, v. 14, suppl., p. 249–252.

_____, 1997a, Theoretical derivation and identification of possible two-layer lizardite polytypes, *in* Merlino, S., ed., Modular aspects of minerals: Budapest, Hungary, Eötvos University Press, EMU Notes in Mineralogy 1, p. 57–80.

_____, 1997b, Structure of the 30-sectored polygonal serpentine. A model based on TEM and SAED studies: Physics and Chemistry of Minerals, v. 24, p. 39–49.

Dódony, I., and Buseck, P. R., 2004a, Lizardite-chlorite structural relationships: An HRTEM study: American Mineralogist, in review.

_____, 2004b, Modeling the chrysotile structures and predicting their experimental data: American Mineralogist, manuscript in preparation.

Dódony, I., Posfai, M., and Buseck, P. R., 2002, Revised structure models for antigorite: An HRTEM study: American Mineralogist, v. 87, p. 1443–1457.

Evans, B. W., 2004, The serpentinite multisystem revisited: Chrysotile is metastable: International Geology Review, v. 46, p. 479–506 (this issue).

Grobéty, B., 2003, Polytypes and higher-order structures of antigorite: A TEM study: American Mineralogist, v. 88, p. 27–36.

Guggenheim, S., and Zhan, W., 1998, Effect of temperature on the structures of lizardite-1T and lizardite-$2H_1$: Canadian Mineralogist, v. 36, p. 1587–1594.

Hanan, B. B., and Sinha, A. K., 1989, Petrology and tectonic affinity of the Baltimore Mafic Complex, Maryland, *in* Mittwede, S. K., and Stoddard, E. F., eds., Ultramafic rocks of the Appalachian piedmont: Geological Society of America Special Paper 231, p. 1–18.

Hess, H. H., 1933, The problem of serpentinization and the origin of certain chrysotile asbestos, talc, and soapstone deposits: Economic Geology, v. 28, p. 634–657.

Hyndman, R. D., and Peacock, S. M., 2003, Serpentinization of the forearc mantle: Earth and Planetary Science Letters, v. 212, p. 417–432.

Hyndman, R. D., Yamano, M., and Oleskevich, D. A., 1997, The seismogenic zone of subduction thrust faults: Island Arc, v. 6, p. 244–260.

Jahanbagloo, I. C., and Zoltai, T., 1968, The crystal structure of a hexagonal Al-serpentine: American Mineralogist, v. 53, p. 14–24.

Krstanovic, I., 1968, Crystal structure of single-layer lizardite: Zeitschrift für Kristallographie Kristallgeometrie Kristallphysik Kristallchemie, v. 126, p. 163–169.

Krstanovic, I., and Karanovic, L., 1995, Crystal structure of 2 lizardites, $Mg_3[Si_2O_5(OH)_4]$: Neues Jahrbuch für Mineralogie-Monatshefte, p. 193–201.

Kunze, W. G., 1956, Die Gewellte Struktur der Antigorits. I: Zeitschrift für Kristallographie, v. 108, p. 82–107.

_____, 1958, Die Gewellte Struktur der Antigorits. II.: Zeitschrift für Kristallographie, v. 110, p. 282–320.

_____, 1961, Antigorit: Fortschritte der Mineralogie, v. 39, p. 206–324.

Lapham, D. M., 1958, Preliminary report on the chromite occurrence at the Wood Mine, Pennsylvania: Pennsylvania Geological Survey Progress Report, 153, 11 p.

Mellini, M., 1982, The crystal structure of lizardite 1T—hydrogen bonds and polytypism: American Mineralogist, v. 67, p. 587–598.

_____, 1986, Chrysotile and polygonal serpentine from the Balangero serpentinite: Mineralogical Magazine, v. 50, p. 301–305.

Mellini, M., and Viti, C., 1994, Crystal structure of lizardite-1T from Elba, Italy: American Mineralogist, v. 79, p. 1194–1198.

Mellini, M., and Zanazzi, P. F., 1987, Crystal structures of lizardite-1T and lizardite-$2H_1$ from Coli, Italy: American Mineralogist, v. 72, p. 943–948.

Mellini, M., Trommsdorff, V., and Compagnoni, R., 1987, Antigorite polysomatism: Behavior during progressive metamorphism: Contributions to Mineralogy and Petrology, v. 97, p. 147–155.

Meyer, C., Leber, M., and Krivanek, O., 1996, Digital micrograph 2.5.7: GATAN Inc.

O'Hanley, D. S., 1996, Serpentinites: Oxford UK, Oxford University Press.

Otten, M. T., 1993, High-resolution transmission electron microscopy of polysomatism and stacking defects in antigorite: American Mineralogist, v. 78, p. 75–84.

Peacock, S. M., 2001, Are the lower planes of double seismic zones caused by serpentine dehydration in subducting oceanic mantle?: Geology, v. 29, p. 299–302.

Peacock, S. M., and Hyndman, R. D., 1999, Hydrous minerals in the mantle wedge and the maximum depth of subduction thrust earthquakes: Geophysical Research Letters, v. 26, p. 2517–2520.

Rucklidge, J. C., and Zussman, J., 1965, Crystal structure of serpentine mineral lizardite $Mg_3Si_2O_5(OH)_4$: Acta Crystallographica, v. 19, p. 381–389.

Schmidt, D., and Livi, K. J. T., 1999, HRTEM and SAED investigations of polytypism, stacking disorder, crystal growth, and vacancies in chlorites from subgreenschist

facies outcrops: American Mineralogist, v. 84, p. 160–170.

Schmidt, M. W., and Poli, S., 1998, Experimentally based water budgets for dehydrating slabs and consequences for arc magma generation: Earth and Planetary Science Letters, v. 163, p. 361–379.

Sharp, T. G., Otten, M. T., and Buseck, P. R., 1990, Serpentinization of phlogopite phenocrysts from a micaceous kimberlite: Contributions to Mineralogy and Petrology, v. 104, p. 530–539.

Spinnler, G. E., 1985, HRTEM study of antigorite, pyroxene-serpentine reactions, and chlorite: Unpubl. Ph.D. thesis, Arizona State University, Tempe, AZ, 248 p.

Staedman, R., and Nuttal, P. M., 1962, The crystal structure of amesite: Acta Crystallographica, v. 15, p. 510–511.

_____, 1963, Polymorphism in cronstedtite: Acta Crystallographica, v. 16, p. 1–8.

_____, 1964, Further polymorphism in cronstedtite: Acta Crystallographica, v. 17, p. 404–406.

Tomeoka, K., and Buseck, P. R., 1985, Indicators of aqueous alteration in CM carbonaceous chondrites: Microtextures of a layered mineral containing Fe, S, O, and Ni: Geochimimica et Cosmochimica Acta, v. 49, p. 2149–2163.

_____, 1990, Phyllosilicates in the Mokoia CV carbonaceous chondrite: Evidence for aqueous alteration in an oxidizing environment: Geochimica et Cosmochimica Acta, v. 54, p. 1745–1754.

Trommsdorff, V., and Connolly, J. A. D., 1996, The ultramafic contact aureole about the Bregaglia (Bergell) tonalite: Isograds and a thermal model: Schweizerische Mineralogische und Petrographische Mitteilungen, v. 76, p. 537–547.

Ulmer, P., and Trommsdorff, V., 1995, Serpentine stability to mantle depths and subduction-related magmatism: Science, v. 268, p. 858–861.

Veblen, D. R., and Buseck, P. R., 1979, Serpentine minerals: Intergrowths and new combination structures: Science, v. 206, p. 1398–1400.

Viti, C., and Mellini, M., 1998, Mesh textures and bastites in the Elba retrograde serpentinites: European Journal of Mineralogy, v. 10, p. 1341–1359.

Wenner, D. B., and Taylor, H. P., Jr., 1974, D/H and O^{18}/O^{16} Studies of serpentinization of ultramafic rocks: Geochimica et Cosmochimica Acta, v. 38, p. 1255–1286.

Whittaker, E. J. W., 1953, The structure of chrysotile: Acta Crystallographica, v. 6, p. 747–748.

_____, 1955a, The diffraction of X-rays by a cylindrical lattice. II: Acta Crystallographica, v. 8, p. 261–265.

_____, 1955b, The diffraction of X-rays by a cylindrical lattice. III: Acta Crystallographica, v. 8, p. 265–271.

_____, 1956a, The structure of chrysotile. II. Clinochrysotile: Acta Crystallographica, v. 9, p. 855–862.

_____, 1956b, The structure of chrysotile. III. Orthochrysotile: Acta Crystallographica, v. 9, p. 862–864.

_____, 1956c, The structure of chrysotile. IV. Parachrysotile: Acta Crystallographica, v. 9, p. 865–867.

Wicks, F. J., and O'Hanley, D. S., 1988, Serpentine minerals: Structures and petrology, *in* Bailey, S. W., ed., Hydrous phyllosilicates (exclusive of micas): Washington, DC, Mineralogical Society of America, Reviews in Mineralogy 19, p. 91–159.

Wicks, F. J., and Whittaker, E. J. W., 1975, A reappraisal of the structures of the serpentine minerals: Canadian Mineralogist, v. 13, p. 227–243.

Wunder, B., Wirth, R., and Gottschalk, M., 2001, Antigorite: Pressure and temperature dependence of polysomatism and water content: European Journal of Mineralogy, v. 13, p. 485–495.

Yada, K., 1967, Study of chrysotile asbestos by a high resolution electron microscope: Acta Crystallographica, v. 23, p. 704–707.

_____, 1971, Study of microstructure of chrysotile asbestos by high resolution electron microscopy: Acta Crystallographica, Section A, v. 27, p. 659–664.

_____, 1979, Microstructures of chrysotile and antigorite by high-resolution electron microscopy: Canadian Mineralogist, v. 17, p. 679–691.

Zhukhlistov, A. P., and Zvyagin, B. B., 1998, Crystal structure of lizardite 1T from electron diffractometry data: Crystallography Reports, v. 43, p. 950–955.

Zvyagin, B. B., 1967, Electron-diffraction analysis of clay mineral structures: New York, NY, Plenum Press, Monographs in Geoscience.

Zvyagin, B. B., Mishchenko, K. S., and Shitov, V. A., 1966, Ordered and disordered polymorphic varieties of serpentine-type minerals and their diagnosis: Soviet Physics Crystallography, USSR, v. 10, p. 539–546.